IEEE Access
Multidisciplinary | Rapid Review | Open Access Journal

Received September 8, 2019, accepted October 3, 2019, date of publication October 21, 2019, date of current version October 31, 2019.

Digital Object Identifier 10.1109/ACCESS.2019.2948735

Additively Manufactured Perforated Superstrate to Improve Directive Radiation Characteristics of Electromagnetic Source

TOUSEEF HAYAT, (Student Member, IEEE), MUHAMMAD U. AFZAL, (Member, IEEE), ALI LALBAKHSH, (Student Member, IEEE), AND KARU P. ESSELLE, (Fellow, IEEE)

Center for Electromagnetic and Antennas Engineering, Faculty of Science and Engineering, Macquarie University, Sydney, NSW 2109, Australia

Corresponding author: Touseef Hayat (touseef.hayat@students.mq.edu.au)

This work was supported by the International Macquarie University Research Excellence Scholarship (iMQRES) Scheme.

ABSTRACT Additively manufactured perforated superstrate (AMPS) is presented to realize directive radio frequency (RF) front-end antennas. The superstrate comprises spatially distributed dielectric unit-cell elements with square perforations, which creates a pre-defined transmission phase delay pattern in the propagating electric field. The proposed square perforation has superior transmission phase characteristics compared to traditionally machined circular perforations and full-wave simulations based parametric analysis has been performed to highlight this supremacy. The AMPS is used with a classical electromagnetic-bandgap resonator antenna (ERA) to improve its directive radiation characteristics. A prototype is developed using the most common, low-cost and easily accessible Acrylonitrile Butadiene Styrene (ABS) filament. The prototype was rapidly fabricated in less than five hours and weighs 139.3 g., which corresponds to the material cost of only 2.1 USD. The AMPS has remarkably improved the radiation performance of ERA by increasing its far-field directivity from 12.67 dB to 21.12 dB and reducing side-lobe level from −7.3 dB to −17.2 dB.

INDEX TERMS Additive manufacturing (AM), acrylonitrile butadiene styrene (ABS), directivity enhancement, perforated dielectric, rapid prototyping, transmission phase shift.

I. INTRODUCTION

The principles of refraction and reflection of electromagnetic waves, implemented through specially designed structures, have been used to develop a range of wave-manipulating artefacts [1]–[4]. An advancement in this regard has been reported recently where the phase of the electric-near field is tailored to enhance the far-field directivity of low-to-medium gain antennas and for steering antenna beam [5]–[7]. The real advantage of performing phase transformation in the near-field region is that the phase-manipulating structure or surface is placed at a sub-wavelength spacing from the electromagnetic radiator and does not greatly increase the maximum height of the overall system [8].

In recent years, almost all of the near-field phase-transforming structures developed for directive radio-frequency (RF) front-end antennas for applications like point-to-point communication and satellite communication are designed using traditional subtractive manufacturing (SM) techniques such as CNC machining or printed circuit board technology [9]–[17]. In SM, pieces of material is removed from a solid block of a dielectric to obtain desired geometry [16]–[18], while PCBs are developed using multiple layers of RF laminates [13]–[15], [19]. The former method is expensive, time consuming, and more importantly requires delicate setup for brittle materials such as ceramics. The material and manufacturing cost associated with multilayered PCBs is at least few hundred dollars even for a moderate size aperture required for medium-gain antennas. A technological solution, considered as a leap forward in manufacturing industry is additive manufacturing (AM), which is also known as 3D printing [20]–[22]. The AM is highly sustainable, easily accessible and environment friendly technique [23], [24], as it involves very little material loss compared to traditional subtractive manufacturing (SM) methods. This advanced manufacturing technique has been tipped as a fail, fast-fail cheap technology, as quick discovery of ideas leads to swift and ideal solutions [25], [26].

The associate editor coordinating the review of this manuscript and approving it for publication was Kai-Da Xu.

The proposed design makes use of AM to develop an extremely low-cost and planar near-field phase transforming structure, which is used as a superstrate of a base antenna and hence referred to as additively manufactured perforated superstrate (AMPS).

In the AMPS, the size of the perforation in a plastic material is varied across the aperture to introduce specific phase distribution pattern into the electric field radiated by a base antenna. The plastic material used for the AMPS is first characterised using dielectric probe kit for RF losses. A unique aspect of AMPS is that it comprises square cylinder perforation (SCP), which are extremely difficult, if not impossible, to sculpt with the traditional SM. Furthermore, introduction of variable perforations in homogenous dielectric to form superstrate, yields a planar geometry which alleviates losses due to shadow blockage observed with non-planar structures used in high-gain applications [17], [27].

The rest of the paper is organized as follows. In Section II, the transmission characteristics of infinitely extended perforated dielectric material is first explained in a unit-cell element type configuration. The effect of perforation on the effective relative permittivity and transmission phase shift of the dielectric material is investigated in Section III. A design example of a porous superstrate is presented in Section IV of the paper. Measured results of the design example are reported in Section V, along with a discussion on the critical parameters of the fabrication process. Finally, a conclusion is given in Section VI.

II. PERFORATED DIELECTRIC

An electromagnetic wave experiences a transmission phase delay when it travels through a medium. In a dielectric medium, the phase delay depends on the relative dielectric constant of the host dielectric material and can be controlled by varying its composition. With a dielectric material having a relative dielectric constant of ε_r, any desired dielectric constant value between ε_0 and ε_r can be achieved by introducing air inclusions or perforation within the dielectric [28], [29]. The perforated dielectric with air is similar to adding air as an impurity in a host dielectric, where the volume of the impurity controls the effective relative permittivity of the resulting material.

The perforation, traditionally, is introduced by drilling holes of various sizes in a dielectric material. The effect of a perforated dielectric strongly depends on the geometry of the perforation, for example the circular and square cylindrical perforations shown in Fig. 1 and Fig. 2, respectively. The two figures show sections of dielectric materials, which are periodically repeating and for this reason are referred to as unit-cell elements following the terminology used in [30]. Each unit-cell element is a square cylinder having a fixed lateral size and height denoted by a and h, respectively.

The first unit-cell element has a circular cylinder perforation (CCP) of diameter b while the second unit-cell element has an SCP perforation of lateral size b. Both perforations run along the length of the unit-cell element, i.e. h(z-axis).

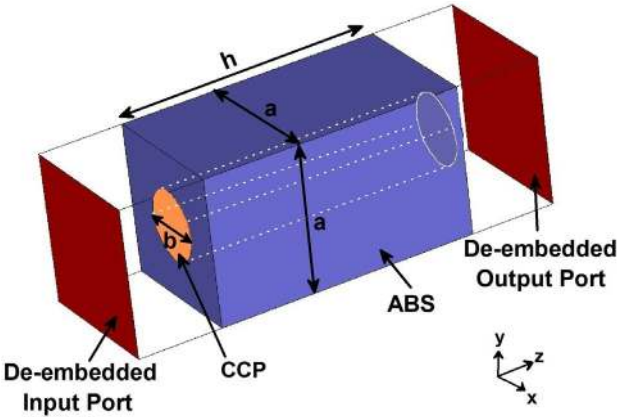

FIGURE 1. A prospective view of a unit-cell element with circular cylindrical perforation.

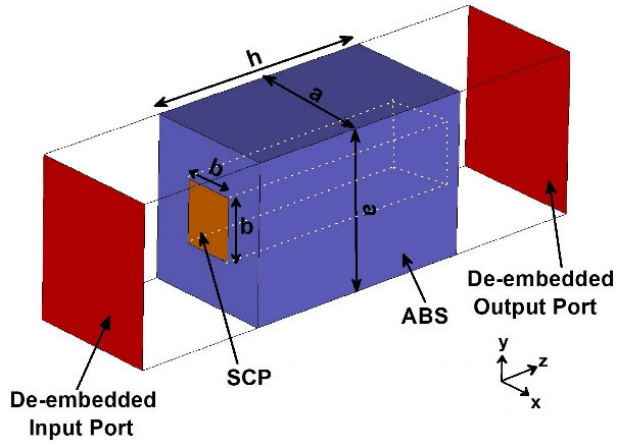

FIGURE 2. A prospective view of a unit-cell element with square cylindrical perforation.

Perforations are named as CCP and SCP because in a plane perpendicular to propagation of electromagnetic wave (xy-plane) they have circular and square shape, respectively. Since the volume of perforation can be varied, the effective dielectric constant of both unit-cell elements along the z-axis can be controlled. Furthermore, the scattering characteristics of perforated dielectric materials can be related and matched to equivalent unperforated homogenous dielectric materials [31]. The parameters of equivalent homogenous dielectric material can be calculated by taking volumetric average of the perforation and the dielectric material in the unit-cell element [15].

For a clear understanding, consider a cross section of a CCP or SCP based unit-cell element in Fig. 3(a) and its equivalent homogenous dielectric in Fig. 3(b). The equivalent effective relative permittivity or ε_{reff} can be calculated using a generic expression:

$$\varepsilon_{reff} = \frac{Dielectric\ vol. \times \varepsilon_d + Perforation\ vol \cdot \times \varepsilon_a}{unit - cell\ vol.} \quad (1)$$

The generic equation (1) can be used to express the effective relative permittivity of a unit-cell element, having CCP and SCP; by calculating the volumes of their perforations

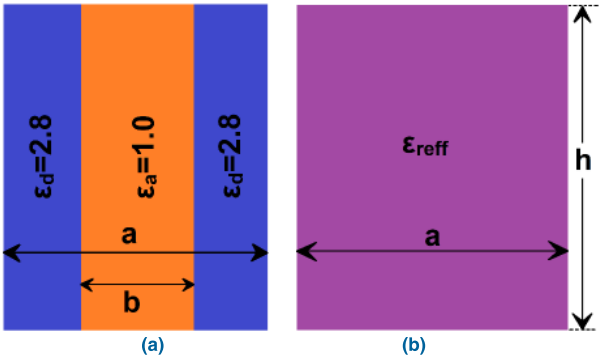

FIGURE 3. (a) Cross-sectional view of non-homogenous perforated unit-cell element. (b) Homogeneous material with effective electromagnetic properties equivalent to non-homogenous unit-cell element.

from physical sizes, it can be expressed for the two cases as

$$\varepsilon_{reff-CCP} = \frac{\left[\left\{(a^2 - \pi\left(\frac{b}{2}\right)^2)\times h\right\}\times\varepsilon_d + (\pi\left(\frac{b}{2}\right)^2 \times h)\times\varepsilon_a\right]}{(a^2 \times h)} \quad (2)$$

$$\varepsilon_{reff-SCP} = \frac{\left[\left\{(a^2 - b^2)\times h\right\}\times\varepsilon_d + (b^2 \times h)\times\varepsilon_a\right]}{(a^2 \times h)} \quad (3)$$

The effect of the perforation type on the $\varepsilon_{\text{reff}}$ value is quantified with specific examples in the following section.

III. PERFORATION SHAPE EFFECT ON MATERIAL CHARACTERISTICS

One of the prime reasons to use AM technology is the limitations of standard machining that has constrained product design for years. Use of AM allows us to build geometries that have been difficult or impossible to fabricate. This includes: modelling of holes that change direction, unrealistic overhangs, or square interior cavities, is now possible and actually simple to construct using 3D printing [32]. Simulation-based comparative analysis was performed for CCP and SCP. A readily available 3D printable dielectric ABS was used for this investigation, which has a relative dielectric constant of 2.8 or $\varepsilon_d = 2.8$. A unit-cell element of lateral size 6.4 mm (or a = 6.4 mm) and height 25 mm (or h = 25 mm) was modelled with periodic boundary conditions in Computer Simulation Technologies (CST) Microwave Studio. The full-wave simulations were used to predict the transmission characteristics of the unit-cell element at the operating frequency of 11.0 GHz.

For CCP and SCP, the lateral dimension of the perforation or b was varied between 0 and 6.4 mm with a step of 0.05 mm. The effective relative permittivity for each of the unit-cell elements is analytically calculated for each step using (2) and (3). Additionally, both unit-cell elements are simulated using periodic-boundary conditions, along the two lateral directions, with CST Microwave Studio. Periodic boundaries were used to characterise transmission of the unit-cell elements for ideal plane-wave transmission. The transmission phase is predicted against the perforation sizes using

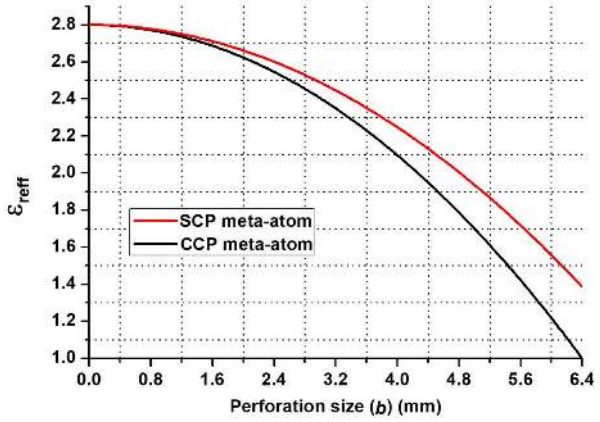

FIGURE 4. Effective relative permittivity comparison of unit-cell elements having SCP and CCP.

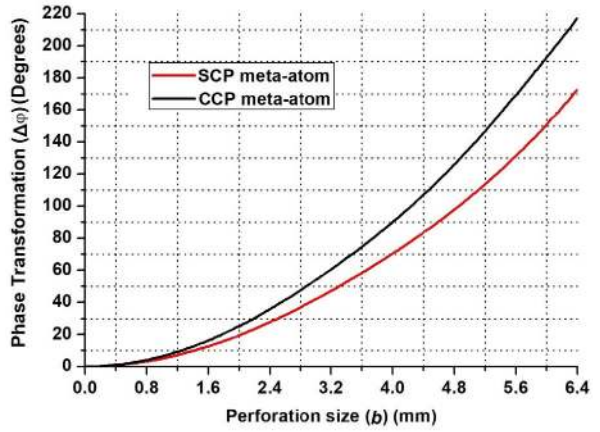

FIGURE 5. Transmission phase shift of unit-cell elements having SCP and CCP.

full-wave simulations. The transmission phase predicted by numerical simulations and the effective relative permittivity values calculated analytically for the two unit-cell elements are plotted in Fig. 4 and Fig. 5, respectively.

For the case when b = a in SCP, the whole region of unit-cell element is occupied with air, hence $\varepsilon_{reff} = \varepsilon_a = 1$. This, however, is not possible with CCP where the lowest achievable effective relative permittivity is 1.39, or $\varepsilon_{reff} = 1.39$. Similarly, the range of transmission phase shift through unit-cell element having SCP is more than that of CCP. It can be observed in Fig. 5 that SCP offers a 217.5° transmission phase shift, compared to CCP with 172.5°. Table 1 compares ε_{reff} and the transmission phase shift offered by both unit-cell elements for various values of b. So, from a parametric study it is evident that, by varying size of perforation through the dielectric block, a transmission phase shift can be achieved, and SCP offers a superior shift compared to other geometries.

The main reason behind the superior transmission phase shift for SCP is that a large perforation volume can be achieved with SCP in a unit-cell element, which results in completely removing dielectric from the unit-cell element. On the other hand, even for the largest perforation size in CCP, there is still dielectric material at the four corners of

TABLE 1. Quantitative comparison of dielectrics having square and circular perforation.

	SCP			CCP		
b (mm)	Vol. perforation (mm^3)	ε_{reff}	$\Delta\varphi$ (deg.)	Vol. perforation (mm^3)	ε_{reff}	$\Delta\varphi$ (deg.)
1.5	51.75	2.70	14.4	40.64	2.72	11.2
3.0	207.0	2.40	53.9	162.5	2.49	41.9
4.5	465.7	1.91	111.4	365.8	2.10	86.9
6.0	828.0	1.22	192.8	650.3	1.56	150.8

the unit-cell element. Because of the ability of SCPs to offer superior phase shift and effective relative permittivity range, they are more suitable for spatial phase-transformation applications. Apart from perforation size, height of unit-cell element is another factor on which phase transformation range is dependent. In this case height of 25 mm was selected because its will suffice to get phase transformation range to realize AMPS which is discussed in next section.

IV. DESIGN EXAMPLE

Although any electromagnetic radiation source can be used to test the performance of AMPS like microstrip-antenna, horn or slot antenna, ERA is considered here, due to its severe phase non-uniformity, and its simple configuration and non-complex feed mechanism. ERAs, are also known as Fabry-Perot cavity antennas, resonant cavity antennas or 2D leaky-wave antennas The classical ERAs comprise a resonant cavity, formed between a ground plane of a feed antenna and a reflecting superstrate [16], [33]. The spacing between the ground plane and the superstrate is set around $\lambda_o/2$, where λ_o is the free-space wavelength, for the cavity to resonate at the operating frequency. In a different approach, fully reflecting surfaces have been proposed to be used in the ERAs's configuration, which can also contribute to a better side-lobe levels as explained in [34], [35].

It is reported that a non-uniform aperture phase distribution in the electric near-field restricts the far-field directivity of classical ERAs despite having a large lateral size [36], [37]. Such an undesirable phenomenon limits the application of ERAs by degrading the antenna's directive radiation characteristics. This sub-optimal directive characteristic can be totally removed by the introduction of AMPS.

A configuration of classical ERA designed to operate at 11 GHz is shown in Fig. 6. The ERA used a printed patch as the feed antenna, having an extended ground plane. An unprinted all-dielectric slab made of Rogers TMM4 ($\varepsilon_r = 4.5$) is used as a partially reflecting superstrate (PRS). It has a thickness of 3.175 mm and it is placed at a spacing of 14.1 mm ($\approx \lambda_o/2$) from the ground plane. The PRS has octagonal geometry with a maximum lateral dimension of 115.2 mm. To quantify the phase non-uniformity on the antenna's aperture, a hypothetical plane named the Input Phase Plane (P-IN) is considered in the nearfield and 8.5 mm above the PRS; this is illustrated in Fig. 6. Hypothetical P-IN can be set at any height as it is introduced to probe phase error on the

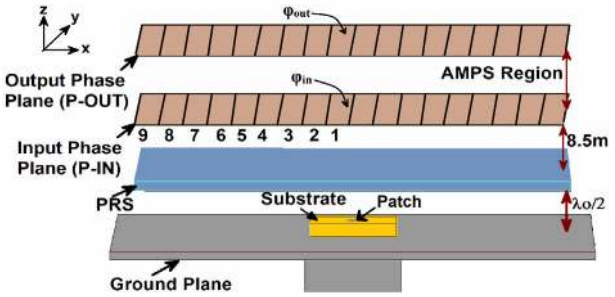

FIGURE 6. A Perspective view of ERA with two hypothetical planes, in the direction of propagation, used for sampling radiated electric field phase. The proposed superstrate is placed between the two hypothetical planes.

aperture of antenna but it should be closer to PRS to reduce overall height of the structure. A parallel plane referred to as the Output Phase Plane (P-OUT) needs to be defined, where a relatively planar phase response is expected after the introduction of the AMPS. A grid of 18 × 18 cells is considered on the P-IN to record the dominant component of the E-field at discrete points above the aperture. The grid size of 18 × 18 elements is chosen to discretize the aperture field distribution of the ERA and depends upon severity of the phase error of antenna. Grid with large inter-element spacing does not accurately quantify the aperture field distribution. Contrary to it, smaller inter-element spacing will result in AMPS with continuous surface, which is relatively complex to fabricate. So particular size of 324 grid elements is chosen which results in intermediate element size, which accurately qualifies the aperture field distribution and is easy to fabricate as well. Each cell in the grid has a square geometry with a size of 6.4 mm ($\approx \lambda_o/4$). The input phase values (φin) are then recorded at the center of each grid cell to calculate the required phase delay. According to the phase data captured in the P-IN, there is an approximate circular symmetry of the phase distribution on the ERA's aperture, so 9 concentric circular arrays of cells are used as 9 phase transformers in the AMPS configuration. The nine phase transformers are then selected using the proposed SCP geometry presented in Section II. To do this, an arbitrary phase value in P-OUT (φ_{out}) is used as a reference phase to quantify the phase error by (9) throughout the aperture. The phase error associated with each of 9 regions will be cancelled by placement of the AMPS between the P-IN and P-OUT. Detailed physical views and analysis of unit-cell element is explained in [8], [9] and is not mentioned here for brevity.

$$\Delta\varphi = \varphi_{out} - \varphi_{in} \tag{4}$$

In (4), $\Delta\varphi$ is calculated by setting φ_{out} to 0 and using φ_{in} as the phase value captured at the centre of each cell in P-IN. Table 2 lists the values of φ_{in} at the centre of each grid cell in the aperture, and the corresponding required transmission phase shift ($\Delta\varphi$) based on which 9 SCP values are selected using Fig. 4. The nine cells are then arranged in a circular manner as shown in in Fig. 7 (a) to realize the AMPS, Fig. 7 (b) illustrates a 3D view of AMPS. The

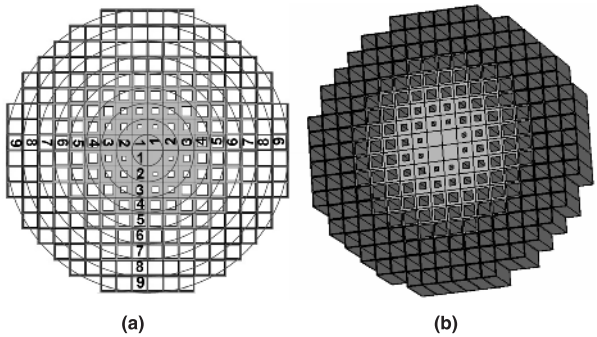

FIGURE 7. The 3D model of the AMPS made of unit-cell elements having SCP (a) top view with concentric circles and (b) perspective view.

TABLE 2. Phase of electric field recorded at P-IN and corresponding perforation sizes required in AMPS.

N	Aperture position (mm)	φ_{in}(deg.)	φ_{in}normalized (deg.)	required$\Delta\varphi$ (deg)	SCP (b) (mm)
1	3.2	22.46	0	0	0
2	9.6	7.68	-14.7	14.7	1.55
3	16	-19.3	-41.7	41.7	2.60
4	22.4	-51.1	-73.5	73.5	3.55
5	28.8	-82.5	-104.9	104.9	4.35
6	35.2	-105.1	-127.5	127.5	4.85
7	41.6	-127.9	-150.3	150.3	5.25
8	48	-153.2	-175.7	175.7	5.75
9	54.4	-139.1	-161.5	161.5	5.45

AMPS is then placed at P-IN. The phase transformation performance of the AMPS can be observed in P-OUT, showing a remarkable improvement on the ERA's phase distribution, where a severe aperture phase error of 175.6° is reduced to 18°, as shown in Fig. 8 and Fig. 9. It has been mentioned earlier that for maximum perforation size ($b = 6.4$ mm), CCP offers transmission phase shift of 172.5°, which is lesser than aperture phase error of ERA under consideration. But using CCP equivalent transmission phase shift can be achieved with perforation size of 5.75 ($b = 5.75$ mm). This highlights superiority of CCP over perforations of other geometries that can be introduced in unit-cell element. After attaining the desired simulation results, the AMPS deign was fabricated using the AM technique.

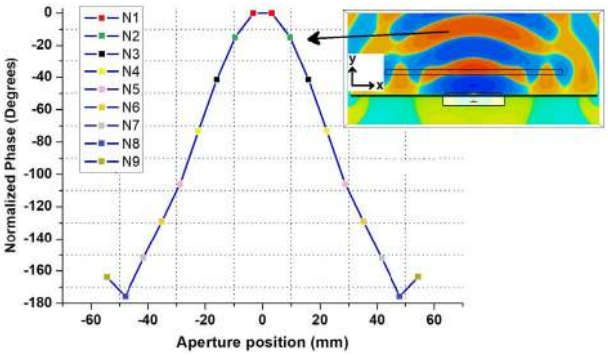

FIGURE 8. The phase of the electric field sampled on the aperture of the ERA without AMPS.

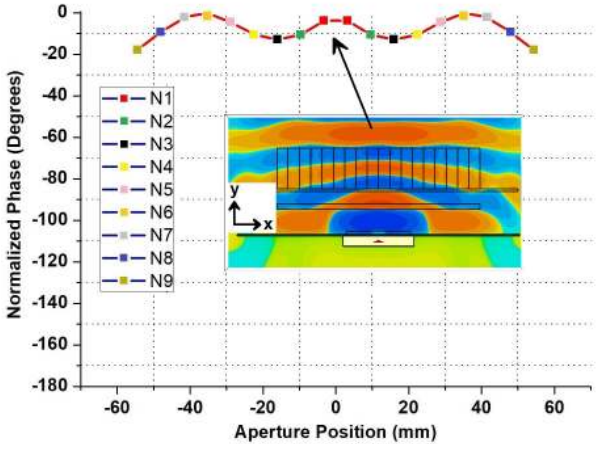

FIGURE 9. The phase of the electric field of ERA with AMPS.

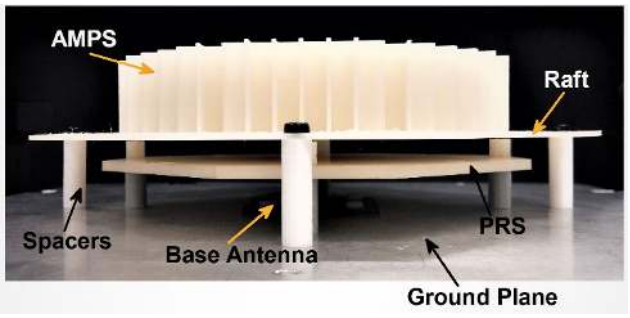

FIGURE 10. A picture of the fabricated AMPS prototype with the ERA.

V. FABRICATION AND MEASUREMENTS

A simulated model was exported as STL file using CST Design Studio for additive manufacturing, and Simplify3D software was used for slicing the imported file. For slicing, layer height was set to 0.2 mm, the bed temperature was fixed to 110°C, the extruder temperature was set as 240°C and an infill percentage of 100% was specified. The sliced file was printed using an Omni3D printer, which offers a heated build plate and a full enclosure feature to withstand environmental changes that can affect the printing process of ABS [38]. The AMPS was printed in less than 5 hours, consuming 55.172 m of 1.75 mm diameter ABS filament. The equivalent plastic weight and cost for this length are 139.34 g and 2.09 USD respectively. It should be mentioned that the same level of gain is achievable using other methods, such as array antennas, which requires feed network. While the conjunction of 3D printing technology with the phase transformation technique does not require auxiliary circuit design and extremely low cost.

The printing time can be significantly reduced by increasing the layer height to the maximum, without sacrificing the AMPS performance. An octagonal raft of a uniform thickness of 2 mm was printed as the base of the AMPS, and four holes were introduced to accommodate spacers that hold the antenna and the AMPS together. A picture of the fabricated prototype of AMPS with ERA is shown in Fig. 10.

To estimate the RF losses in the AMPS, the ABS material was characterised using an Agilent 85070e dielectric probe

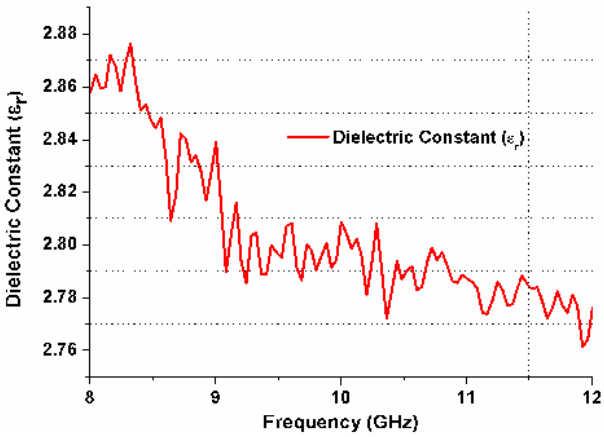

FIGURE 11. Measured dielectric constant of the ABS sample using the dielectric-probe kit method.

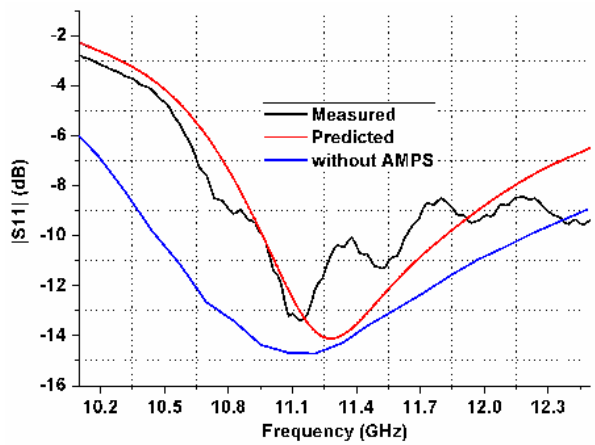

FIGURE 12. Input reflection coefficients with and without AMPS.

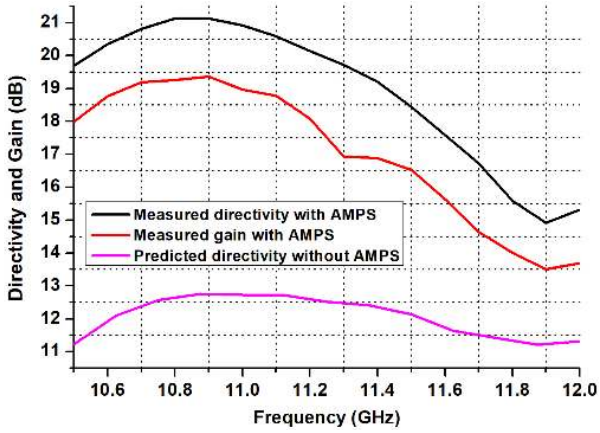

FIGURE 13. Variation of predicted and measured peak directivity and gain in the operating frequency band.

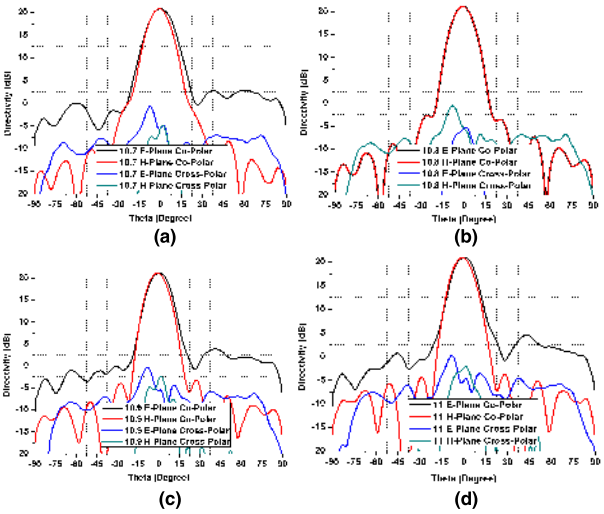

FIGURE 14. Farfield directivity patterns of the ERA with AMPS along E-plane and H-plane at frequencies: (a) 10.7 GHz (b) 10.8 GHz (c) 10.9 GHz and (d) 11.0 GHz.

kit. For the characterisation, a cylinder having a 20 mm diameter and a height of 15 mm was printed out of ABS using above mentioned print settings. The sample was characterized within a frequency range of 1 to 20 GHz. The plots of dielectric constant for the printed samples in the frequency band are given in Fig. 11. At the operating frequency of 11 GHz, the dielectric constant (ε_r) is 2.78, which is very close to the value reported for ABS in the literature [39].

Measurements were performed in an NSI spherical near-field chamber. The measured results of the AMPS with the ERA are in a reasonable agreement with the results predicted by simulations. The predicted and measured input reflection coefficients are shown in Fig. 12. The measured 10 dB return loss bandwidth is 6.5%, from 10.8 GHz to 11.63 GHz. A drastic improvement in the radiation patterns of the antenna has been achieved as a result of the introduction of the AMPS. The measured peak far-field gain and directivity within the operating frequency band are plotted in Fig. 13. The figure indicates that the highest measured directivity of 21.12 dBi is achieved at 10.9 GHz, but was 12.63 dBi without the AMPS. The far-field directivity patterns taken at four different frequencies for co- and cross polarization within the operating band are given in Fig. 14. At 11 GHz, even the largest side-lobe is below −2.5 dBi and is around 17dB less than the beam peak. The quality of the pattern in terms of beam shape, side-lobe level, and 3dB beam-width is excellent at the other three sampled frequencies shown in Fig. 14.

VI. CONCLUSION

A low-cost and light-weight additively manufactured perforated superstrate with SCPs has been presented for ERA. The square perforations is nearly impossible to carve with traditional machining methods and can be easily done using additive manufacturing. SCPs have been used because they offer wider range of effective relative permittivity and transmission phase shift. The fabrication of superstrate takes five hours even with 100% infill density. The electromagnetic properties in terms of improving directivity of ERA is comparable to previously reported designs with added advantages of low-cost and rapid prototyping.

REFERENCES

[1] H. D. Hristov, J. M. Rodriguez, and W. Grote, "The grooved-dielectric Fresnel zone plate: An effective terahertz lens and antenna," *Microw. Opt. Technol. Lett.*, vol. 54, no. 6, pp. 1343–1348, Jun. 2012.

[2] W. Pan, C. Huang, M. Pu, X. Ma, J. Cui, B. Zhao, and X. Luo, "Combining the absorptive and radiative loss in metasurfaces for multi-spectral shaping of the electromagnetic scattering," *Sci. Rep.*, vol. 6, no. 1, Aug. 2016, Art. no. 21462.

[3] N. T. Nguyen, N. Delhote, M. Ettorre, D. Baillargeat, L. Le Coq, and R. Sauleau, "Design and characterization of 60-GHz integrated lens antennas fabricated through ceramic stereolithography," *IEEE Trans. Antennas Propag.*, vol. 58, no. 8, pp. 2757–2762, Aug. 2010.

[4] A. Arbabi, E. Arbabi, Y. Horie, S. M. Kamali, and A. Faraon, "Planar metasurface retroreflector," *Nature Photon.*, vol. 11, no. 7, pp. 415–420, Jul. 2017.

[5] M. Ettorre, S. Bruni, G. Gerini, A. Neto, N. Llombart, and S. Maci, "Sector PCS-EBG antenna for low-cost high-directivity applications," *IEEE Antennas Wireless Propag. Lett.*, vol. 6, pp. 537–539, 2007.

[6] A. Lalbakhsh, M. U. Afzal, and K. P. Esselle, "Multiobjective particle swarm optimization to design a time-delay equalizer metasurface for an electromagnetic band-gap resonator antenna," *IEEE Antennas Wireless Propag. Lett.*, vol. 16, pp. 912–915, 2016.

[7] M. U. Afzal and K. P. Esselle, "Steering the beam of medium-to-high gain antennas using near-field phase transformation," *IEEE Trans. Antennas Propag.*, vol. 65, no. 4, pp. 1680–1690, Apr. 2017.

[8] T. Hayat, K. P. Esselle, M. U. Afzal, and K. Singh, "3D printed all dielectric phase correcting surface for resonant cavity antenna," in *Proc. IEEE Asia–Pacific Conf. Antennas Propag. (APCAP)*, Aug. 2018, pp. 214–215.

[9] M. Asaadi and A. Sebak, "Gain and bandwidth enhancement of 2×2 square dense dielectric patch antenna array using a holey superstrate," *IEEE Antennas Wireless Propag. Lett.*, vol. 16, pp. 1808–1811, 2017.

[10] B. Majumder, K. Kandasamy, and K. P. Ray, "A zero index based metalens loaded wideband directive antenna combined with reactive impedance surface," *IEEE Access*, vol. 6, pp. 28746–28754, 2018.

[11] L. Kong, S. Yan, and G. A. E. Vandenbosch, "Directive planar antenna array fed by dielectric waveguide for WiFi applications," *Microw. Opt. Technol. Lett.*, vol. 60, no. 8, pp. 1963–1967, Aug. 2018.

[12] C. Mateo-Segura, A. Dyke, H. Dyke, S. Haq, and Y. Hao, "Flat Luneburg lens via transformation optics for directive antenna applications," *IEEE Trans. Antennas Propag.*, vol. 62, no. 4, pp. 1945–1953, Apr. 2014.

[13] M. U. Afzal, K. P. Esselle, and A. Lalbakhsh, "A metasurface to focus antenna beam at offset angle," in *Proc. 2nd URSI Atlantic Radio Sci. Meeting (AT-RASC)*, May/Jun. 2018, pp. 1–4.

[14] M. U. Afzal, A. Lalbakhsh, and K. P. Esselle, "A low-profile beam-tilted antenna array for receiving direct-broadcast satellite services," in *Proc. IEEE Asia–Pacific Conf. Antennas Propag. (APCAP)*, Aug. 2018, pp. 147–148.

[15] R. K. Arya, S. Pandey, and R. Mittra, "A technique for designing flat lenses using artificially engineered materials," in *Proc. IEEE Antennas Propag. Soc. Int. Symp. (APSURSI)*, Jul. 2014, pp. 769–770.

[16] A. Lalbakhsh, M. U. Afzal, K. P. Esselle, S. L. Smith, and B. A. Zeb, "Single-dielectric wideband partially reflecting surface with variable reflection components for realization of a compact high-gain resonant cavity antenna," *IEEE Trans Antennas Propag.*, vol. 67, no. 3, pp. 1916–1921, Mar. 2019.

[17] A. Petosa, A. Ittipiboon, and S. Thirakoune, "Array of perforated dielectric Fresnel lenses," in *Proc. URSI Int. Symp. Electromagn. Theory (EMTS)*, Pisa, Italy, 2004, pp. 969–971.

[18] M. U. Afzal, K. P. Esselle, and B. A. Zeb, "Dielectric phase-correcting structures for electromagnetic band gap resonator antennas," *IEEE Trans. Antennas Propag.*, vol. 63, no. 8, pp. 3390–3399, Aug. 2015.

[19] A. Lalbakhsh and K. P. Esselle, "Design of an improved resonant cavity antenna," in *Proc. 19th Int. Conf. Electromagn. Adv. Appl. (ICEAA)*, 2017, pp. 1658–1660.

[20] H. Lipson and M. Kurman, *Fabricated: The New World of 3D Printing*. Hoboken, NJ, USA: Wiley, 2013.

[21] A. J. Capel, R. P. Rimington, M. P. Lewis, and S. D. R. Christie, "3D printing for chemical, pharmaceutical and biological applications," *Nature Rev. Chem.*, vol. 2, no. 12, pp. 422–436, Dec. 2018.

[22] T. Hayat, M. U. Afzal, A. Lalbakhsh, and K. P. Esselle, "3-D-printed phase-rectifying transparent superstrate for resonant-cavity antenna," *IEEE Antennas Wireless Propag. Lett.*, vol. 18, no. 7, pp. 1400–1404, Jul. 2019.

[23] E. Canessa, C. Fonda, M. Zennaro, and N. Deadline, "Low-Â-Cost 3D printing for science, education and sustainable development," in *Proc. 1st Int. Workshop (ICTP)*, May 2013, p. 1.

[24] S. Mueller, S. Im, S. Gurevich, A. Teibrich, L. Pfisterer, F. Guimbretiere, and P. Baudisch, "WirePrint: 3D printed previews for fast prototyping," in *Proc. 27th Annu. ACM Symp. User Interface Softw. Technol.*, Oct. 2014, pp. 273–280.

[25] Z. Liu, M. Zhang, B. Bhandari, and Y. Wang, "3D printing: Printing precision and application in food sector," *Trends Food Sci. Technol.*, vol. 69, pp. 83–94, Nov. 2017.

[26] J. D. Prince, "3D printing: An industrial revolution," *J. Electron. Resour. Med. Libraries*, vol. 11, no. 1, pp. 39–45, Mar. 2014.

[27] A. Petosa and A. Ittipiboon, "Shadow blockage effects on the aperture efficiency of dielectric Fresnel lenses," *IEE Proc.—Microw., Antennas Propag.*, vol. 147, no. 6, pp. 451–454, Dec. 2000.

[28] A. Petosa and A. Ittipiboon, "Design and performance of a perforated dielectric Fresnel lens," *IEE Proc.—Microw., Antennas Propag.*, vol. 150, no. 5, pp. 309–314, Oct. 2003.

[29] A. Petosa, A. Ittipiboon, and S. Thirakoune, "Investigation on arrays of perforated dielectric Fresnel lenses," *IEE Proc.—Microw., Antennas Propag.*, vol. 153, no. 3, pp. 270–276, Jun. 2006.

[30] R. K. Arya, "Meta-atoms and artificially engineered materials for antenna applications," in *Developments in Antenna Analysis and Design*, vol. 1. Edison, NJ, USA: IET, 2018, pp. 351–405.

[31] M. Kadic, G. W. Milton, M. van Hecke, and M. Wegener, "3D metamaterials," *Nature Rev. Phys.*, vol. 1, no. 3, pp. 198–210, Mar. 2019.

[32] G.-L. Huang, S.-G. Zhou, C.-Y.-D. Sim, T.-H. Chio, and T. Yuan, "Lightweight perforated waveguide structure realized by 3-D printing for RF applications," *IEEE Trans. Antennas Propag.*, vol. 65, no. 8, pp. 3897–3904, Aug. 2017.

[33] M. U. Afzal and K. P. Esselle, "Improving phase uniformity in the aperture: A method to enhance radiation characteristics of Fabry–Perot resonator antennas," in *Proc. IEEE Int. Symp. Antennas Propag. USNC/URSI Nat. Radio Sci. Meeting*, Jul. 2015, pp. 39–40.

[34] K. Dutta, D. Guha, and C. Kumar, "Theory of controlled aperture field for advanced superstrate design of a resonance cavity antenna with improved radiations properties," *IEEE Trans. Antennas Propag.*, vol. 65, no. 3, pp. 1399–1403, Mar. 2017.

[35] K. Dutta, D. Guha, and C. Kumar, "Synthesizing aperture fields over the superstrate of resonance cavity antenna for modifying its radiation properties," *IEEE Antennas Wireless Propag. Lett.*, vol. 15, pp. 1677–1680, 2016.

[36] R. M. Hashmi and K. P. Esselle, "A class of extremely wideband resonant cavity antennas with large directivity-bandwidth products," *IEEE Trans. Antennas Propag.*, vol. 64, no. 2, pp. 830–835, Feb. 2016.

[37] A. Lalbakhsh, M. U. Afzal, K. P. Esselle, and S. L. Smith, "Wideband near-field correction of a Fabry–Perot resonator antenna," *IEEE Trans. Antennas Propag.*, vol. 67, no. 3, pp. 1975–1980, Mar. 2019.

[38] B. D. Gesner, "Environmental surface effects on ABS resins," *J. Appl. Polym. Sci.*, vol. 9, no. 11, pp. 3701–3706, Nov. 1965.

[39] B. Riddle, J. Baker-Jarvis, and J. Krupka, "Complex permittivity measurements of common plastics over variable temperatures," *IEEE Trans. Microw. Theory Techn.*, vol. 51, no. 3, pp. 727–733, Mar. 2003.

TOUSEEF HAYAT received the B.S. degree in telecommunication engineering from the University of Engineering and Technology, Taxila, Pakistan, the M.S. degree (Hons.) from the National University of Sciences and Technology (NUST), Islamabad, Pakistan, and the Master of Research (MRes) degree (Hons.) in electronics engineering from Macquarie University, Australia, in 2018. He is currently pursuing the Ph.D. with Macquarie University. His research interests include electromagnetic-bandgap resonant antennas, additive manufacturing of microwave components, phase and amplitude transforming metasurfaces, and dielectric characterization. He received several prestigious awards, including the International Research Training Program Scholarship (iRTP) for the MRes and International Macquarie University Research Excellence Scholarship (iMQRES) for his Ph.D. degree.

MUHAMMAD U. AFZAL (S'13–M'16) received the B.S. degree in electronics engineering (Hons.) and the master's degree in computational science and engineering from the National University of Sciences and Technology (NUST), Islamabad, Pakistan, in 2005 and 2011, respectively, and the Ph.D. degree in electronics engineering from Macquarie University, in 2016.

From 2010 to 2012, he was a Lab Engineer with the Samar Mubarakmand Research Institute of Microwave and Millimeterwave Studies (SMRIMMS), Islamabad, Pakistan. From 2012 to 2013, he was a Lecturer with the Electrical Engineering Department, NUST, Islamabad. He is currently a Research Associate with the Engineering Department, Macquarie University. His research interests include electromagnetic band gap or Fabry-Perot resonator antennas, high-gain planar metasurface-based antennas, radial-line slot antennas, phased arrays, free-standing phase-shifting structures or metasurfaces, frequency selective surfaces, near-field phase transformation, and far-field pattern synthesis using near-field phase transformation.

Dr. Afzal received the NUST Merit Base Scholarship during his undergraduate studies and the International Macquarie Research Excellence Scholarship (iMQRES) for his Ph.D. studies.

ALI LALBAKHSH received the B.S. and M.S. degrees in electronic and telecommunication engineering from Islamic Azad University, Iran, in 2008 and 2011, respectively, and the Master of Research (HD) degree in electronics engineering from Macquarie University, Australia, in 2015. He is currently pursuing the Ph.D. degree with Macquarie University. From 2011 to 2015, he was a Lecturer with Islamic Azad University, Kermanshah, Iran. His research interests include resonance-based antennas, frequency selective surfaces, periodic and electromagnetic band gap structures, evolutionary optimization methods, and microwave passive components. He received several prestigious awards, including the International Research Training Program scholarship (iRTP) for his MRes degree, International Macquarie University Research Excellence Scholarship (iMQRES) for his Ph.D. degree, the Commonwealth Scientific and Industrial Research Organization (CSIRO) grants on Astronomy and Space exploration, the Macquarie University Postgraduate Research Fund (PGRF), and the WiMed Travel Support Grants. He was a recipient of the 2016 ICEAA-IEEE APWC Cash Prize as well as first and third prices of the IEEE Region 10 Student Paper Contest, postgraduate category, in 2018 and 2016, respectively.

KARU P. ESSELLE (M'92–SM'96–F'16) received the B.Sc. degree (Hons.) in electronic and telecommunication engineering from the University of Moratuwa, Sri Lanka, and the M.A.Sc. and Ph.D. degrees, with near-perfect GPA, in electrical engineering from the University of Ottawa, Canada.

He was the Director of the WiMed Research Centre and an Associate Dean - Higher Degree Research (HDR) of the Division of Information and Communication Sciences and also the Director of the Centre for Collaboration in Electromagnetic and Antenna Engineering at Macquarie University. He has served as a member of the Dean's Advisory Council and the Division Executive and as the Head of the Department for several times. He is currently a Distinguished Professor in electromagnetic and antenna engineering with the University of Technology Sydney and also a Visiting Professor of Macquarie University, Sydney. He has authored approximately 600 research publications and his articles have been cited over 8,400 times. In 2018, his publications received 1084 citations. He is the first Australian Antenna Researcher ever to reach Google Scholar h-index of 30 and his citation indices have been among the top Australian antenna researchers for a long time (in October 2019: i10 is 164 and h-index is 43). Since 2002, his research team has been involved with research grants, contracts, and Ph.D. scholarships worth over 18 million dollars, including 15 Australian Research Council grants, without counting the 245 million-dollar SmartSat Corporative Research Centre, which started, in 2019. His research has been supported by many national and international organizations, including Australian Research Council, Intel, US Air Force, Cisco Systems, Hewlett-Packard, the Australian Department of Defence, the Australian Department of Industry, and the German and Indian governments. He has provided expert assistance to more than a dozen companies, including Intel, Hewlett Packard Laboratory, USA, Cisco Systems, USA, Audacy, USA, Cochlear, Optus, ResMed, and Katherine-Werke, Germany. Among them, his team designed the high-gain antenna system for the world's first entirely Ka-band CubeSat made by Audacy, USA, and launched to space by SpaceX, in December 2018. This is believed to be the first Australian-designed high-gain antenna system in space, since CSIRO-designed antennas in Australia's own FedSat launched, in 2002. According to a Special Report published by The Australian national newspaper, in 2019, he is the "National Research Field Leader" in microelectronics and electronic packaging fields in engineering discipline as well as the electromagnetism field in the disciplines of physics and mathematics. He is with the College of Expert Reviewers of the European Science Foundation (2019–2022) and he has been invited to serve as an International Expert/Research Grant Assessor by several other research funding bodies as well, including European Research Council and national agencies in The Netherlands, Canada, Finland, Hong-Kong, Georgia, South Africa, and Chile. He has been invited by vice-chancellors of Australian and overseas universities to assess applications for promotion to professorial levels. He has also been invited to assess grant applications submitted to Australia's most prestigious schemes, such as Australian Federation Fellowships and Australian Laureate Fellowships.

Dr. Esselle was elevated to prestigious IEEE Fellow grade for his contributions to resonance-based antennas. He is also a Fellow of the Engineers Australia. He received the awards, including the 2004 Innovation Award for best invention disclosure, the 2009 Vice Chancellor's Award for Excellence in Higher Degree Research Supervision, the 2011 Outstanding Branch Counsellor Award from IEEE headquarters (USA), the 2012 Engineering Excellence Awards for Best Published Paper from IESL NSW Chapter, the 2017 Certificate of Recognition from the IEEE Region 10, in 2016, the 2017 Excellence in Research Award from the Faculty of Science and Engineering, the 2017 Engineering Excellence Award for Best Innovation, the 2017 Highly Commended Research Excellence Award from Macquarie University, the 2019 Motohisa Kanda Award from IEEE-USA, for the most cited article in the IEEE TRANSACTIONS ON ELECTROMAGNETIC COMPATIBILITY in the past five years, the selection as a Finalist for the forthcoming 2019 Macquarie University Research Excellence Awards for Innovative Technologies, and the 2019 ARC Discovery International Award. His mentees have been awarded many fellowships, awards, and prizes for their research achievements. Forty-eight international experts who examined the theses of his recent Ph.D. graduates ranked them in the top 5% or 10%. In 2018 and 2019, he has been selected to Chair the prestigious Distinguished Lecturer Program Committee of the IEEE Antennas and Propagation (AP) Society - the premier global learned society dedicated for antennas and propagation - which has about 9,000 members worldwide. After two stages in the selection process, he was selected by this society as one of two candidates in the ballot for 2019 President of the Society. Only three people from Asia or Pacific apparently have received the Honor in the 68-year history of this society. He was also one of the three Distinguished Lecturers (DL) selected by the society, in 2016. He is the only Australian to Chair the AP DL Program ever, the only Australian AP DL in almost two decades, and the second Australian AP DL ever (after UTS Distinguished Visiting Professor Trevor Bird). He has been continuously serving the IEEE AP Society Administrative Committee in several elected or ex-officio positions, since 2015. He is also the Chair of the Board of management of Australian Antenna Measurement Facility, and was the elected Chair of IEEE New South Wales (NSW), and IEEE NSW AP/MTT Chapter, in 2016 and 2017, respectively. He is currently the Technical Program Committee Co-Chair of ISAP 2015, APMC 2011, and TENCON 2013, and the Publicity Chair of the ICEAA 2016, IWAT 2014, and APMC 2000. In addition to the large number of invited conference speeches he has given, he has been an invited keynote speaker of several IEEE and URSI conferences and workshops, including URSI'19 Seville, Spain, and 23rd ICECOM, in 2019 in Dubrovnik, Croatia. He is an Associate Editor of the IEEE TRANSACTIONS ON ANTENNAS AND PROPAGATION and IEEE ACCESS. His previous research activities are posted in the web at http://web.science.mq.edu.au/ esselle/.